Water Research 229 (2023) 119515

Contents lists available at ScienceDirect

Water Research

journal homepage: www.elsevier.com/locate/watres

Spatiotemporal variability and controlling factors of indirect N_2O emission in a typical complex watershed

Jie Liang *, Wenzhuo Tang, Ziqian Zhu, Shuai Li, Kang Wang, Xiang Gao, Xin Li, Ning Tang, Lan Lu, Xiaodong Li

College of Environmental Science and Engineering, Hunan University and Key Laboratory of Environmental Biology and Pollution Control, Hunan University, Ministry of Education, Changsha 41082, PR China

ARTICLE INFO

Keywords:
Indirect N_2O emission
Spatiotemporal pattern
Controlling factors
SWAT
PLS-SEM

ABSTRACT

The mechanisms of N_2O emissions from inland rivers remain poorly understood because of the high variability of dissolved N_2O concentration and the complexity of influencing factors. Thus, it is necessary to research the spatiotemporal patterns and influencing factors to understand the driving mechanisms of riverine N_2O emissions. We combine the Soil and Water Assessment Tool (SWAT) outputs with established empirical equations to identify the spatiotemporal fluctuations of riverine N_2O emissions and evaluate model performance through field measurements in a typical watershed. The spatiotemporal hotspots of N_2O emissions are then determined, and the relative importance of environmental variables is further determined by correlation and attribution analysis. The results indicate that the riverine N_2O emissions are relatively high from August to October, which accounted for 35.38% of the annual emissions. Temporal changes are attributed to agricultural activities and meteorological factors. Agricultural activities such as planting and fertilization lead to increased diffuse nitrogen loads on the land surface. Meantime, heavy precipitation events enhance the transport of nutrients, resulting in changes in nitrogen levels in the river. Spatial analysis shows that the urban watersheds (191.22 ± 156.19 μmol m^{-2} d^{-1}) are the hotspots of riverine N_2O emission, which are 1.55–3.03 times that of non-urban rivers. Spatial variations are mainly affected by riverine physicochemical indicators for different watersheds. Sewage from various sources received by urban rivers provides appropriate environmental conditions for N_2O production, and transports large exogenous dissolved N_2O. Furthermore, salinity ($r = 0.80$; $p < 0.001$) and nitrogen nutrients in riverine physicochemical indicators show a significant correlation with N_2O fluxes. It emphasizes that N-related (TN, NH_4^+, NO_3^-) indicators are important reactants for N_2O generation, which can promote nitrification and denitrification. Meanwhile, the results of structural equation modeling (SEM) also demonstrate that N_2O emissions follow a similar pattern to riverine dissolved N_2O concentration ($r = 0.841$, $p < 0.001$), and non-point source ($r = 0.678$, $p < 0.001$) play an important role in the changes of dissolved N_2O concentrations. Our results highlight that certain hot moments and hot spots of rivers play a disproportionate role in year-round and basin-wide N_2O emissions, respectively. It is necessary to implement more effective management measures by controlling key environmental factors to reduce N_2O emissions.

1. Introduction

Nitrous oxide (N_2O), as one of the powerful greenhouse gases (GHGs), is an important contributor to climate change with a global warming potential 265 times that of carbon dioxide (CO_2) (Song et al., 2022). The atmospheric concentration of N_2O has steadily increased from 270 ppb since the mid-18th century to 335 ppb in 2022 due to the recent great increase in human activities (Lan et al., 2022). This steady increment is primarily attributable to direct emissions from soils caused by agricultural activities (Huang et al., 2022). Furthermore, some nitrogen from agricultural activities can be transported via leaching and surface runoff, thereby promoting N_2O generation and emissions from aquatic systems (Chen et al., 2015). These off-site emissions are considered indirect N_2O emissions (Wang et al., 2022). Anthropogenic sources are estimated to account for 38.5% (2.7–11.1 Tg y^{-1}) of global N_2O emissions, of which 10–17% (0.68–0.9 Tg y^{-1}) are from inland

* Corresponding author.
E-mail address: liangjie@hnu.edu.cn (J. Liang).

https://doi.org/10.1016/j.watres.2022.119515
Received 13 October 2022; Received in revised form 13 December 2022; Accepted 18 December 2022
Available online 19 December 2022

rivers (Wang et al., 2021). Among the river ecosystems, N_2O emission flux (μg N_2O – N m^{-2} h^{-1}) followed these principles: subtropical rivers (median = 26.5 ± 334.0) > temperate rivers (median = 25.2 ± 554.4) > tropical rivers (median = 11.8 ± 204.0) (Li et al., 2021). Compared with other ecosystems, the spatiotemporal patterns of N_2O emissions from subtropical rivers have considerable variability (Hu et al., 2016). In addition, given the high variability of N_2O and the complexity of influencing factors, more studies emphasize the necessity of better quantifying the contributions of various driving factors to the spatiotemporal pattern in riverine N_2O emissions (Zhao and Zhang, 2021). Hence, identifying hotspots of N_2O emissions and exploring the impacts of driving factors on riverine N_2O emissions have important implications for reducing N_2O emissions.

Currently, most research of riverine N_2O emissions at the basin scale has been conducted through air-water gas exchange models, chambers or process-based models (Fu et al., 2018). However, specific site experiments and monitoring are difficult for evaluating the spatiotemporal pattern of riverine N_2O emissions at the catchment scale because of low spatiotemporal sampling resolutions and high variability of dissolved N_2O concentration. Therefore, watershed-scale models are a powerful method for assessing the spatiotemporal pattern in riverine N_2O emissions (Gao et al., 2020). Soil and Water Assessment Tool (SWAT) is a process-based model at the watershed scale that simulates hydrological, nutrient, and biogeochemical cycles. The official version of SWAT cannot simulate riverine N_2O emissions, but previous studies have demonstrated the feasibility of using SWAT as a framework to study the spatiotemporal fluctuations of N_2O emissions. By far, SWAT-DayCent (daily CENTURY), SWAT-N_2O, SWAT-GHG, SWAT-MKT (Microbial kinetics and thermodynamic), and SWAT-N_2O coupler were developed to simulate N_2O emissions at the catchment scale by integrating the SWAT model with biogeochemical processes or empirical models or both (Bhanja et al., 2019; Gao et al., 2019; Shrestha et al., 2018; Wagena et al., 2017; Wu et al., 2016; Yang et al., 2017). However, the above models focus on N_2O emissions from the soil instead of N_2O emissions from river networks at the watershed scale. Recently, Gao et al. (2020) established a riverine dissolved N_2O concentration model with different dissolved inorganic N (DIN = $[NH_4^+]$ + $[NO_3^-]$) levels based on observations collected from different regions. The dissolved N_2O concentration model and dynamic atmospheric N_2O concentration algorithm were integrated into SWAT to develop SWAT-F_{N2O}. SWAT-F_{N2O} achieved acceptable performance in mid-to-high latitude agricultural watersheds (Gao et al., 2020). However, we found some differences between the simulated and observed values of dissolved N_2O concentrations during practical application because of the high spatial heterogeneity of dissolved N_2O concentrations. In addition, Marzadri et al. (2017) proposed a process-based parsimonious model at the watershed scale, but this model neglected the effect of diffuse nitrogen from the land surface (Gao et al., 2020; Marzadri et al., 2020). Some global N_2O models containing surface hydraulics information have been developed (Marzadri et al., 2020; Tian et al., 2020; Yao et al., 2020), but the contribution of benthic and hyporheic are not well described (Marzadri et al., 2021). The power law scaling model parameterized riverine N_2O emissions using two denitrification Damköhler numbers (Marzadri et al., 2020), but this model ignored N_2O input outside the channel (Hu et al., 2021a). The recent application of machine learning methods in the environmental domain has achieved satisfactory results. However, due to the scarcity of local environment variables and available N_2O data, using existing algorithms to directly simulate riverine N_2O emissions may cause poor forecasts (Marzadri et al., 2021).

The production of N_2O in rivers is considered to be controlled by different environmental factors interacting in complicated ways. The driving factors of N_2O emission can be divided into local factors and regional factors (Grossel et al., 2021). Local factors dominate microbial processes at the microscopic scale, mainly including water environmental factors and stream hydraulics (Quick et al., 2016). Regional factors can significantly influence local factors at the macro scale, usually determined by large-scale environmental changes (Grossel et al., 2021). Regional factors mainly include pollution sources, meteorological factors, and land use. Temporally, monthly N_2O emission fluxes are influenced by seasonal cycles of transport velocities and the concentration gradient of N_2O. These changes are primarily controlled by meteorological changes and non-point source effects (Gao et al., 2020). Spatially, the N_2O emissions rates of different watershed landscapes are significantly different. Land use is a multifaceted reflection of riverine characteristics, incorporating those that can considerably impact N_2O production (e.g., microbial processes, river chemistry, and riverbed morphology) (Zhang et al., 2020a).

Regional factors and local factors are not independent of each other but are related. The relative importance of different driving factors to N_2O emissions remains unclear (Soued et al., 2016). Existing studies to identify driving factors of N_2O emissions typically used single factor or simple regression analysis, while attribution analysis methods based on observational data are scarce (Qin et al., 2020). Recently, attribution analysis methods represented by structural equation modeling (SEM) are being used to visually distinguish the effects of environmental variables (Liang et al., 2021). The SEM takes into account not only the direct impacts of environmental factors on research objectives, but also the interplay among various factors. The pathway model helps to clarify the relationship between environmental variables and N_2O emission fluxes, and the established SEM can quantify the relative contributions of various driving factors (Zhao and Zhang, 2021). The partial least squares (PLS) SEM is one of the SEM models. Compared with traditional SEM, it has less stringent requirements on the amount of data and normal distribution (Hair et al., 2012). To further explore the interaction of regional factors and local factors, we decoupled the environmental variables utilizing SEM.

The Liuyang River Basin (LYRB) is located in the subtropical monsoon climate region in central China, and has a distinct seasonal pattern of hydrology and meteorology. Meanwhile, LYRB is dominated by forest, agriculture, and urban areas from upstream to downstream according to the different landscapes of the basin. Therefore, the spatiotemporal patterns are more representative and the meteorological and hydrological effects are more significant when the LYRB is taken as the study area for the study on riverine N_2O emissions. Specifically, the main goals of this study are to (i) assess the spatiotemporal patterns of N_2O emissions using a combination of SWAT output results and established empirical equations, (ii) find the temporal and spatial hotspots of N_2O emissions and identify the main factors affecting the spatiotemporal patterns, and to (iii) explore the relative contribution of environmental factors to N_2O emission fluxes.

2. Materials and methods

2.1. Study area

Liuyang River is the second-class tributary of Yangtze River, with a watershed area of 4665 km^2 and a total length of 222 km. The LYRB is located in central China and has a subtropical climate. The average temperature is about 17.4 °C, and the annual rainfall is around 1601.1 mm. The altitude of the LYRB ranges from −14 to 1603 m, and the terrain is high in the northeast and low in the southwest (Fig. 1).

The main land use types of the LYRB are forestland, cropland, urban, and water. In order to reveal the magnitude of N_2O emission and further compare the emission hotspots of different types of rivers, we defined the ranked 20% watersheds according to the percentage of land use as urban watersheds (UW, %urban ≥ 20%), agricultural watersheds (AW, %cropland ≥ 25%), and forest watersheds (FW, %forest ≥ 75%) in order. The remaining watersheds were determined as mixed watersheds (MW, %forest < 75%& %cropland < 25%&% urban < 20%) (Zhang et al., 2020a, 2021) (Fig. S1).

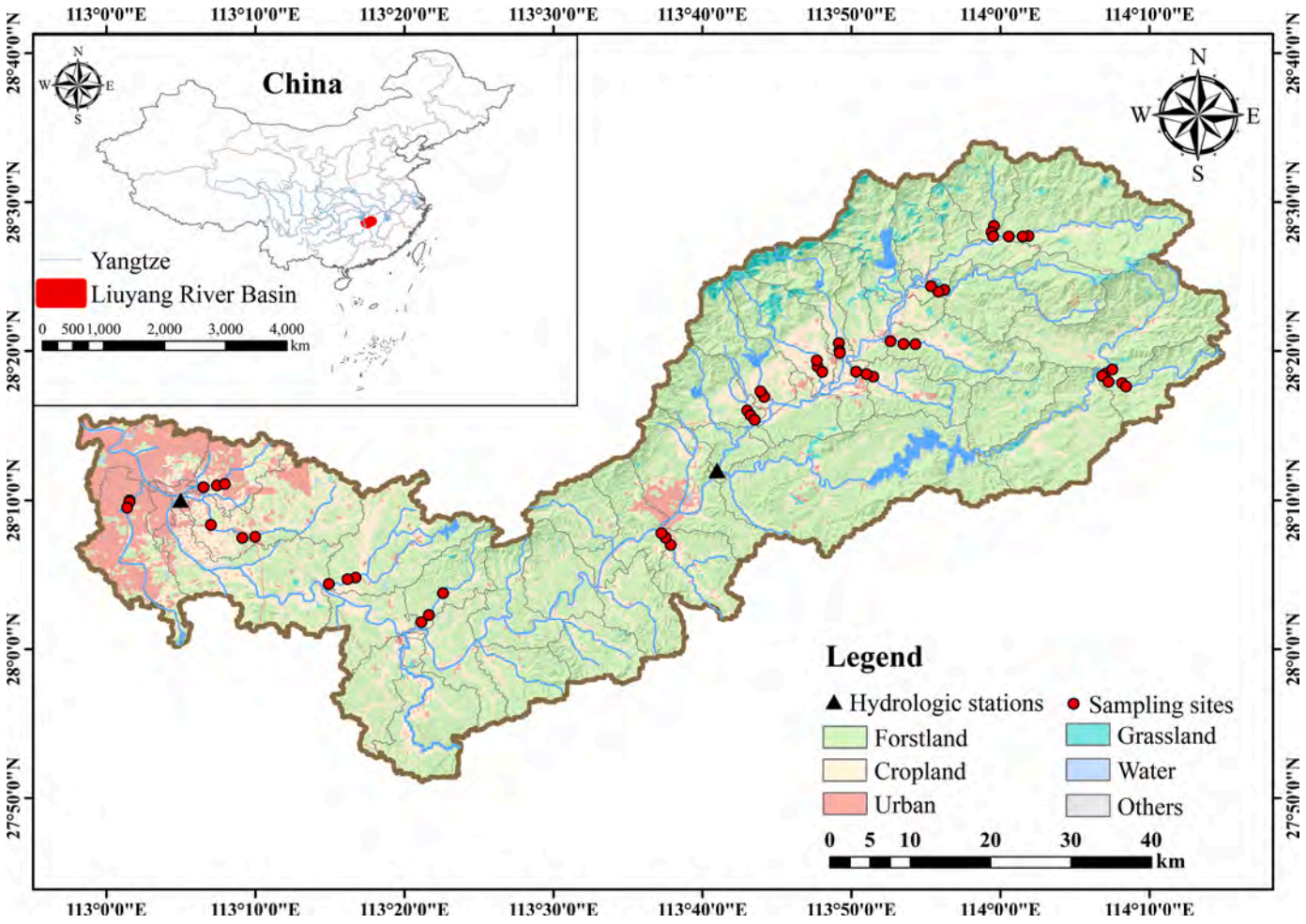

Fig. 1. Location of the study area and sampling sites in Liuyang River Basin.

2.2. Data sources

We chose fifty-one sampling sites along the Liuyang River in January 2021 and July 2021 according to the proportion of various land use types in the whole watershed (Fig. 1). Of the 51 sites, 21, 6, 6, and 18 of them were collected in forest rivers, agricultural rivers, urban rivers, and mixed rivers, respectively (Table S1). A total of 15 environmental variables were measured. The pH, dissolved oxygen (DO) and water temperature (WT) were measured *in situ* (HQ2200, HACH, USA). At the same time, 4 × 250 mL river surface water was collected for further laboratory measurements to determine total phosphorous (TP), total nitrogen (TN), ammonia nitrogen (NH_4^+), nitrate nitrogen (NO_3^-), chloridion (Cl^-), and sulfate ion (SO_4^{2-}). All these environmental variables were measured based on the standard methods.

For N_2O analysis, water samples were slowly poured into the sample vials and overflowed several volumes of water after flooding the sample vials while preventing bubbles during the draining process. Afterwards, 200 μL of $HgCl_2$ (0.5% v/v final concentration) was injected to the samples to restrain microbial activity. Then they were stored in a low-temperature environment and returned them to the laboratory to determine dissolved N_2O in the water samples by headspace equilibrium techniques (Agilent 7890B, μECD) (Wang et al., 2018).

The input basic data for the SWAT model included Digital Elevation Model (DEM), land use, soil, and weather data, and types and sources of the SWAT model data were summarized in Table S2. Meanwhile, we intended to assess the drivers of N_2O emissions in the watershed and thereby compiled some of the environmental factors which have been previously documented or predicted to potentially affect N_2O emissions at the watershed scale (Ghimire et al., 2020; Yao et al., 2020). The environmental factors are listed in Table S3, including land use, water quality, point source, non-point source, and meteorological factors. We screened the observed variables in different types of factors by indicator loadings. Theoretically indicator loadings should be greater than 0.700. However, indicator loadings of 0.400 to 0.700 are satisfactory when the average variance extracted (AVE) is greater than 0.500 (Table S6) (Hair et al., 2012; Hulland, 1999).

2.3. N_2O emissions fluxes for rivers

The riverine N_2O emissions model consists of the following modules:

(i) The air-water gas exchange model was used as the framework for modeling riverine N_2O emissions (Wang et al., 2020). Riverine N_2O emissions fluxes were calculated by the water-air gas exchange, which is dependent on the N_2O transfer velocity, and the air-water N_2O concentration gradient (Wang et al., 2020), as follows:

$$F_{N_2O} = K_{N_2O}\left([N_2O]_{water} - [N_2O]_{eq}\right) \quad (1)$$

where F_{N_2O} is the riverine N_2O emissions fluxes across the water-atmosphere interface (μmol m^{-2} d^{-1}); K_{N_2O} is the transfer velocity of N_2O (m d^{-1}); $[N_2O]_{water}$ and $[N_2O]_{eq}$ represent concentrations of dissolved N_2O (nmol L^{-1}) in the surface water and theoretical equilibrium concentration (nmol L^{-1}), respectively.

(ii) The dissolved N_2O concentration model was developed according to principal reactants ($[NH_4^+]$ and $[NO_3^-]$) of the N_2O cycling. We collected individual measurements of global rivers to build the training dataset, which were obtained from different regions according to the previous literature (Table S4). The outliers (DIN concentrations and dissolved N_2O concentrations) that were more than 1.5 times the interquartile range from upper quartile or lower quartile were cleaned in the training dataset (Hellerstein, 2008). The training dataset includes 230 observations in Asia, 231 observations in Europe, 295 observations in Africa, and 8 observations in North America. Dissolved N_2O concentrations demonstrated a powerful correlation with the $[NH_4^+]$ and $[NO_3^-]$ concentrations than with $[NH_4^+]$ or $[NO_3^-]$ concentrations individually (Gao et al., 2020). $[N_2O]_{water}$ was calculated as the equation of the riverine $[NH_4^+]$ and $[NO_3^-]$ concentrations based on training dataset. Urban, agricultural and forested rivers represent different N levels that may exhibit different responses to dissolved N_2O concentrations (Mwanake et al., 2019). Therefore, we split the training dataset according to different N levels to explore the response of dissolved N_2O concentration to different N levels. The empirical function of dissolved N_2O and DIN ($[NH_4^+]$ and $[NO_3^-]$) in rivers was established by using multiple linear regression according to different N levels. The R^2 values of dissolved N_2O concentration and DIN were 0.61 (DIN < 6 mg L^{-1}) and 0.74 (DIN > 6 mg L^{-1}), respectively (Fig. 2).

$$[N_2O]_{water} = 2.92[NO_3^-] + 24.23[NH_4^+] + 12.28 \quad (DIN < 6\ mg/L) \tag{2}$$

$$[N_2O]_{water} = 0.79[NO_3^-] + 22.36[NH_4^+] + 14.74 \quad (DIN > 6\ mg/L) \tag{3}$$

where $[NH_4^+]$ and $[NO_3^-]$ are the riverine ammonia and nitrate concentrations (mg/L), respectively.

Dissolved N_2O concentration module performance was evaluated through field measurements. Dissolved N_2O in the on-site water samples was calculated by the headspace equilibrium technique (Wang et al., 2018), as following Eq. (4):

$$C_{obs} = P\left(K_0 + \frac{1}{RT}\frac{V_g}{V_l}\right) \tag{4}$$

where C_{obs} is the dissolved N_2O concentration (mol L^{-1}); P represents the partial pressure of N_2O (atm) in the headspace after equilibration; K_0 represents the solubility coefficient (mol L^{-1} atm^{-1}) calculated according to the temperature and salinity (Weiss and Price, 1980); R represents the gas constant (L atm mol^{-1} K^{-1}); T represents temperature (K) when equilibrating; V_l and V_g represent the volume of the water samples and the gas phase (L), respectively.

(iii) Since N_2O emissions are affected by multiple factors and their interactions, a process-based model which can incorporate these components is required for realistic simulations. The SWAT model includes processes such as hydrology, nutrient cycles, and management practices and can incorporate possible aspects that affect N_2O emissions (Ghimire et al., 2020). Meanwhile, SWAT can model the riverine NH_4^+, NO_3^-, and water temperature and provide information about the stream hydraulics. These parameters are needed to simulate watershed-scale riverine N_2O emissions (Fu et al., 2018). Table S2 data were used as input for the SWAT model. Then SWAT-CUP was used to calibrate and validate the model parameters related to streamflow and N load simulations (Liang et al., 2020). Finally, the riverine DIN concentration was determined based on the calibrated SWAT model.

(iv) The theoretical equilibrium N_2O concentration model for the study area was calculated according to the atmospheric N_2O data from the Global Monitoring Laboratory (GML) (https://gml.noaa.gov/hats/combined/N2O.html) considering atmospheric N_2O dynamic (Gao et al., 2020) (Fig. S2); (More details were provided in the Supplementary material)

(v) The N_2O transfer velocity module was calculated based on the combination of both wind and water currents. We applied hydromorphological equations to quantify the stream features of the river (Raymond et al., 2012) (Fig. S3). (More details were provided in the Supplementary material)

2.4. Data analysis method

2.4.1. Spatiotemporal analysis method

Heatmap (Fig. 3a) and box-and-whisker diagrams (Fig. 3b,c) of the spatiotemporal distribution of N_2O fluxes were plotted by Origin 2020b (version 9.75). To further identify the hot and cold spots of N_2O emissions, we performed hotspot analysis based on the Hot Spot Analysis (Getis-Ord Gi*) tool in ArcGIS (version 10.8) (Fig. S4). This tool has been widely acknowledged as a powerful tool for visually identifying spatial clusters of statistically significant hot (high values) or cold (low values) spots within a study area (Jana and Sar, 2016). Meanwhile, we used Locally weighted scatterplot smoothing (Lowess) to further explore the relationship between land use and emission flux. For data with a certain trend, Lowess can fit a line that conforms to the overall trend, and then analyze the relationship between variables (Zhang et al., 2021).

2.4.2. Correlation and attribution analysis

To study the impact of environmental factors on N_2O emissions, we

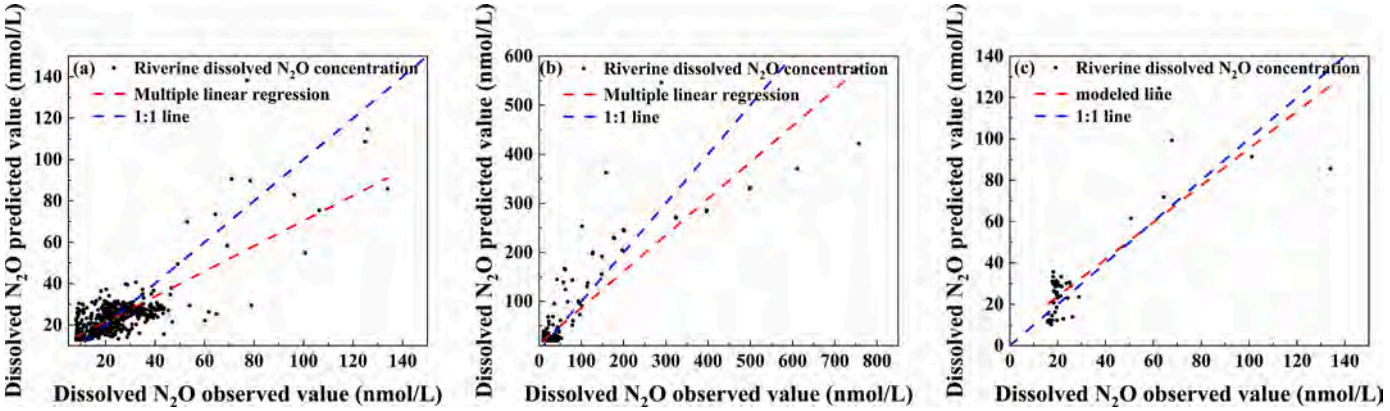

Fig. 2. Multiple linear regression relationship between the observed and predicted dissolved riverine N_2O concentrations during the training for low (a) and high (b) nitrogen concentrations. Comparison of the modeled and observed riverine dissolved N_2O concentrations during the testing (c).

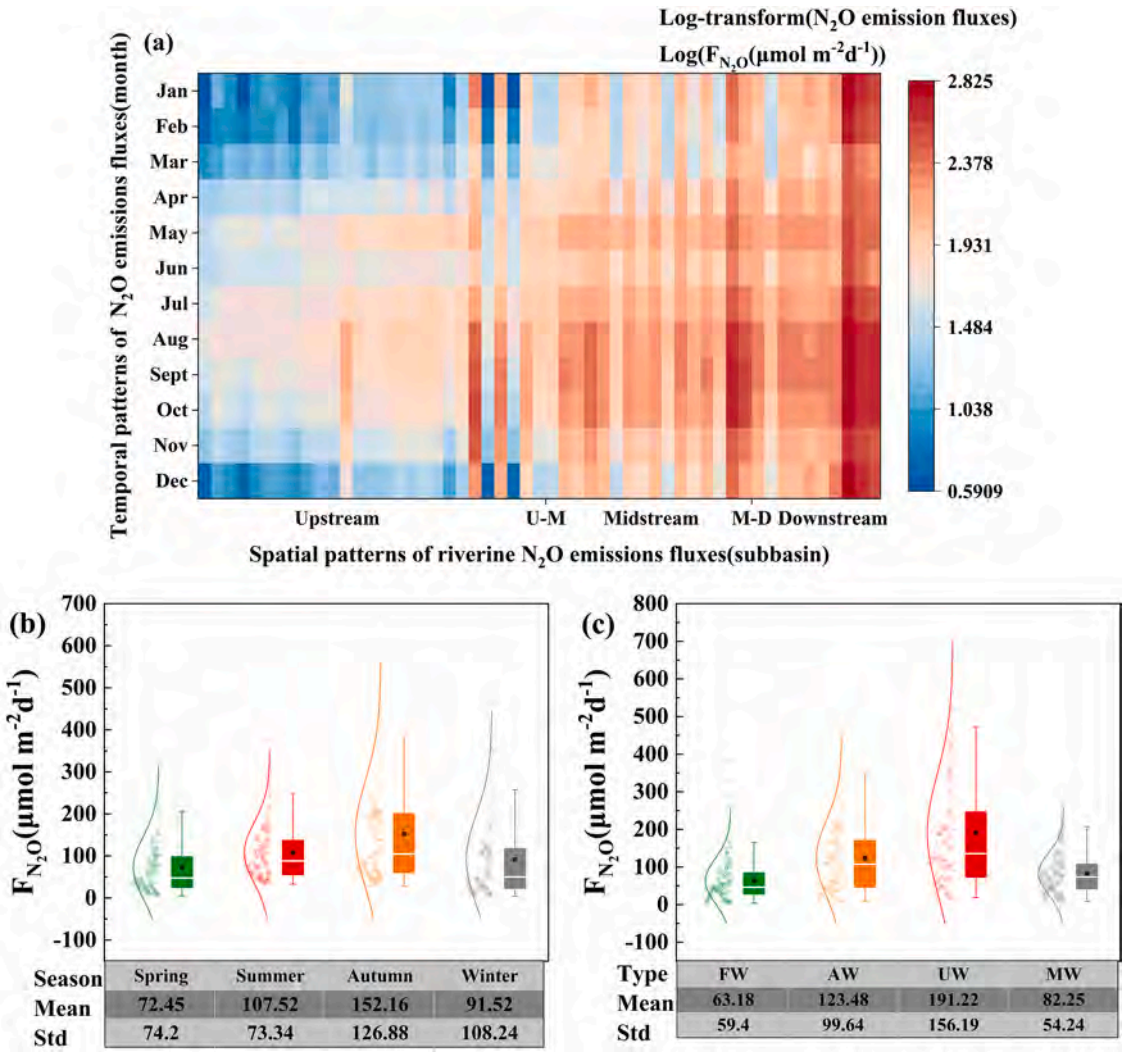

Fig. 3. Spatiotemporal characteristics of monthly mean riverine N_2O emission fluxes simulated in the sub-basin. (a)Heatmap of log-transformed N_2O emission fluxes for different months and subbasins. The abscissa corresponds to the spatial emission patterns of upstream, midstream and downstream, and the ordinate corresponds to the temporal emission patterns of different months. Box-and-whisker diagrams represent the variation of riverine N_2O emissions fluxes for different (b) seasonal and (c) watersheds. The whisker diagrams on the left show the scatter and its corresponding distribution curve, and the box diagrams on the right indicate to the range from 25 to 75%. Whiskers correspond to the range of 2.5–97.5%, and the median and mean are represented by horizontal white lines and black squares, respectively.

calculated the correlations among variables using Correlation Plots in Origin 2020b (version 9.75). To further determine the driving force of environmental factors on N_2O emissions, we integrated a path model with SEM to reveal the direct and indirect impacts of key explanatory variables on N_2O fluxes (Zhao and Zhang, 2021). Given the data characteristics of this study (small sample size and non-normal data) and the model complexity, we used the partial least squares (PLS) method to determine the path coefficients and model fitting parameters by SmartPLS (version 3.3.9). Finally, we conduct an overall assessment of the PLS-SEM model through the reflective measurement models evaluation and the structural model evaluation. The evaluation criteria of the reflective measurement models mainly include indicator reliability (indicator loadings), internal consistency (Cronbach's alpha (CA) and composite reliability (CR)), convergent validity, and discriminant validity (Fornell-Larcker criterion and HTMT) (Hair et al., 2012; Henseler et al., 2015; Urbach and Ahlemann, 2010). The evaluation criteria of structural model mainly include Coefficient of determination (R^2), Effect size (f^2), Path Coefficient (t&p values) and Goodness of Fit (GOF) (Hair et al., 2012; Khan et al., 2021; Urbach and Ahlemann, 2010). The reflective measurement models and structural model achieved satisfactory performance, indicating that the PLS-SEM has been well established and can be utilized for further analysis. (detailed evaluation criteria and model performance are supplied in the Supplementary Information)

3. Results and discussion

3.1. Model performance evaluation

After the sensitivity analysis using SWAT-CUP, the monthly discharge, ammonia, and nitrate were calibrated and validated from the two hydrology monitoring stations in the LYRB. Table S5 listed the sensitive parameters adopted in the SWAT model. R^2 and NS for calibration and validation periods were calculated to assess the model simulation performance. For streamflow, NH_4^+-N loading and NO_3^--N loading simulations, the R^2 values and NS values during calibration and validation were greater than 0.65 and 0.60, respectively (Fig. S5). Thus, the model performance met the requirements, which meant that the SWAT model has been well established in the LYRB and can be utilized for further analysis (Yang et al., 2016). For different N levels, the R^2

values of dissolved N_2O concentration and DIN were 0.61 (DIN < 6 mg L^{-1}) and 0.74 (DIN > 6 mg L^{-1}), respectively. The riverine dissolved N_2O concentration module achieved acceptable performance during the testing stages ($R^2 = 0.68$) (Fig. 2), indicating that the developed module can capture the spatiotemporal variability of dissolved N_2O concentration for different reaches. Considering the atmospheric N_2O dynamic, the R^2 values for predicting the monthly atmospheric N_2O concentration in the study area were all greater than 0.99, demonstrating that the annual average monthly growth rate was fairly constant (Fig. S2). In conclusion, the magnitude and spatiotemporal patterns of riverine N_2O emissions fluxes can be well captured by coupling the SWAT model and the riverine N_2O emissions model.

3.2. Spatiotemporal pattern of riverine N_2O emissions fluxes

3.2.1. Cultivation period is the hotspot of riverine N_2O emissions

Riverine N_2O emission fluxes for different seasons are presented in Fig. 3b, which has strong temporal variability. The dissolved N_2O concentrations were far above theoretical equilibrium concentrations, indicating that the supersaturation of N_2O in rivers was significant. Specifically, the average fluxes of riverine N_2O can be ranked as: autumn (152.16 ± 126.88 μmol m^{-2} d^{-1}) > summer (107.52 ± 73.34 μmol m^{-2} d^{-1}) > winter (91.52 ± 108.24 μmol m^{-2} d^{-1}) > spring (72.45 ± 74.2 μmol m^{-2} d^{-1}). The strong riverine N_2O emissions from August to October are the hot spots in the whole year, accounting for about 35.38% of the annual emission. Among them, the N_2O flux in September was the highest, with its average flux (156.84 ± 148.15 μmol m^{-2} d^{-1}) of 1.87–2.50 times that of the fluxes from February to April.

Temporal patterns of subtropical inland watersheds (Fig. 4) are dominated by the combined effects of gas transfer velocity and the concentration gradient of N_2O. The temporal variability of dissolved N_2O concentration (Fig. 4b) is controlled by both local and regional factors. July to October is the cultivation period of single rice and late rice in the LYRB (Liu et al., 2015). The diffuse nitrogen loads on the land surface increased sharply due to the effects of plant and fertilization during this period (Huang et al., 2022). In the meantime, heavy precipitation events enhanced the transport of nutrients, resulting in increasing nitrogen levels in rivers (Yao et al., 2020). Nitrogen is an important reactant for N_2O generation, which can promote nitrification and denitrification. The gas transfer velocity and theoretical equilibrium concentration changes are mainly controlled by regional factors. Gas transfer velocity (Fig. 4c) generally depends on seasonal changes in meteorological and hydrological conditions (Yan et al., 2022). The LYRB is located in the subtropical monsoon climate region, which has an obvious seasonal pattern of hydrology and meteorology. The rainy season (April to August) precipitation accounted for 60.4% of the annual precipitation. The increase in water velocity and depth caused by heavy precipitation promoted the gas diffusing effect across the water-air interface (Song et al., 2022). The theoretical equilibrium N_2O concentration (Fig. 4d) was mainly affected by the air temperature. From June to September, the water temperature reached the highest value in the whole year under the influence of air temperature. The fugacity of N_2O took on a descending trend with increasing water temperature. Low fugacity and moderate atmospheric N_2O content resulted in lower theoretical equilibrium N_2O concentration (Gao et al., 2019; Weiss and Price, 1980). Consequently, the riverine N_2O emissions from August to October are the hot spots in the whole year under the influence of high N_2O transfer velocity and N_2O concentration difference.

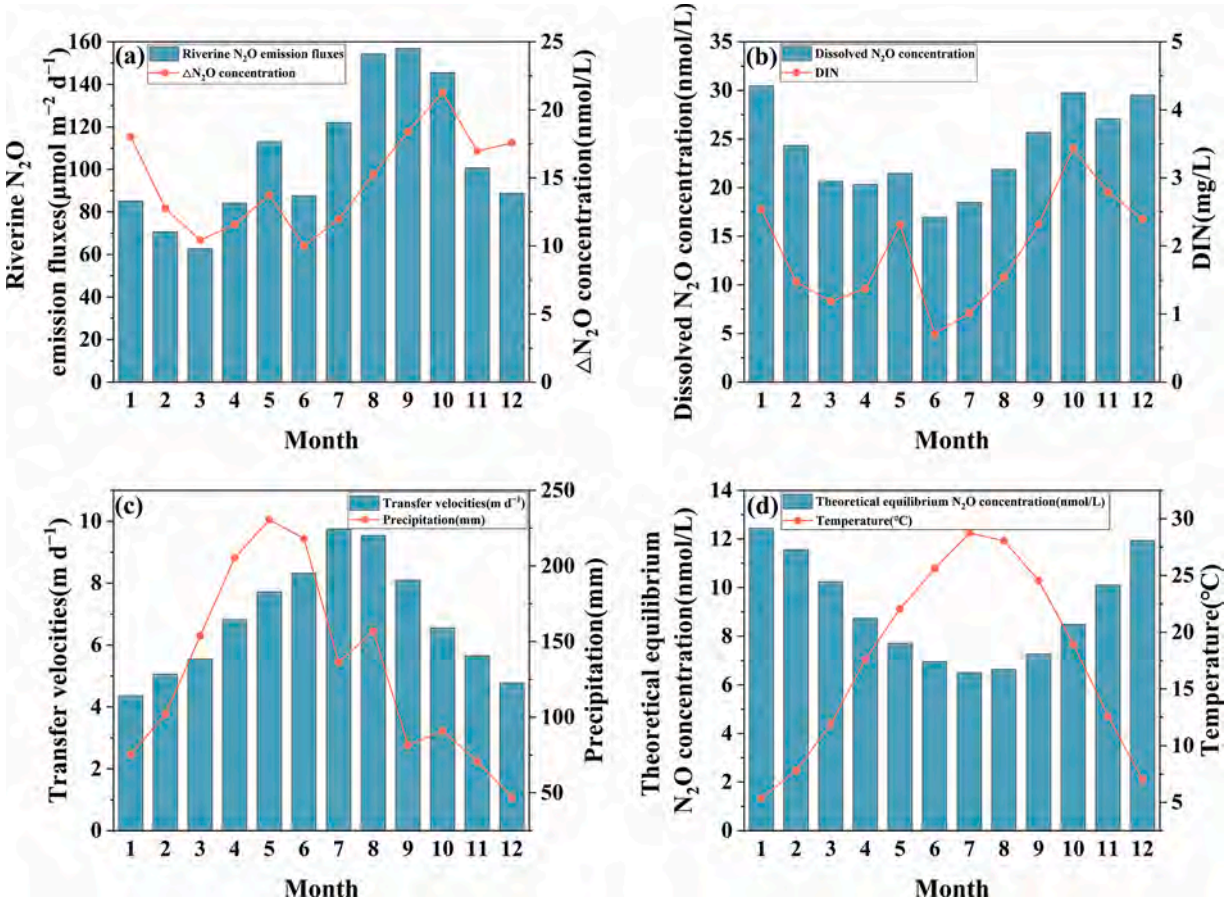

Fig. 4. Modeled monthly N_2O emission fluxes and (a) ΔN_2O concentration, (b) dissolved N_2O concentration, (c) transfer velocities, (d) theoretical equilibrium N_2O concentration.

3.2.2. Urban watersheds are hotspots of indirect N_2O emission

The discrepancies in the riverine physicochemical indicators (Table 1) caused by variations of land use types (Table S13) may be the potential factor across watersheds for the differences in magnitudes of the N_2O emissions (Zhang et al., 2020a, 2021). The flux of N_2O at each reach was significantly correlated with the dominant land use and its percentage within the watershed (Fig. 5). Although urban rivers, as hotspots of riverine N_2O emissions, only account for 18.46% of the channel area in the whole basin, N_2O emissions from urban reach account for 27.93% of the annual mean N_2O emissions (Table S14). This illustrates that UW (10.95 kg $N_2O - N\ yr^{-1}$) played a disproportionate role in basin-wide N_2O emissions (Fig. 5a) (Borges et al., 2015). Specifically, the differences in pollution sources, water environmental factors, and activities of certain microorganisms and critical enzymes in different types of watersheds caused the significantly higher N_2O (191.22 ± 156.19 μmol $m^{-2}\ d^{-1}$) in UW than in other river segments (He et al., 2017; Quick et al., 2019; Zhou et al., 2022). UW frequently receive substantial wastewater from point-source discharges (mean: UW = 61142.07 m^3/d > AW = 58945.99 m^3/d > MW = 328.07 m^3/d > FW = 156.97 m^3/d) and urban runoff, with much higher nutrient loadings than other rivers. Sewage from various sources provides appropriate environmental conditions for N_2O production in rivers (He et al., 2017; Yu and Lu, 2018). Exogenous dissolved N_2O in sewage from wastewater treatment plants is another important source of riverine N_2O emissions in urban waters besides *in-situ* N_2O generation (Zhou et al., 2022). Therefore, the spatial hotspots of N_2O emission commonly appear in river segments where considerable sewage is discharged (Turner et al., 2016).The abundant presence of specific substances and inconstant riverine physicochemical conditions may inhibit the activities of critical enzymes and certain microorganisms. Hydrogen sulfide (H_2S), which is highly present in UW, strongly restrains the reduction of N_2O to N_2, contributing to more N_2O accumulation (Quick et al., 2019; Zhang et al., 2020a). The average *in-situ* water temperature in UW was slightly higher than in others due to warm sewage from households and industries and urban heat island effects. Consequently, nitrifying and denitrifying microorganisms could adequately take advantage of favorable thermal conditions to promote more N_2O production (Venkiteswaran et al., 2014).

The N_2O emissions demonstrated intense spatial heterogeneity in the LYRB, and there was a visible pattern from upstream to downstream. FW had the lowest N_2O fluxes (63.18 ± 59.40 μmol $m^{-2}\ d^{-1}$), which were 23–67% lower than others. Specifically, the reasons why FW are cold spots for N_2O emissions are as follows: Firstly, FW have limited N supply and oversaturated DO compared with others, resulting in weak processes related to N_2O production (Borges et al., 2018). Second, the mismatch of forms of reactive nitrogen (Nr) with DO conditions is not conducive to N_2O generation. Incomplete denitrification is normally facilitated by elevated nitrate concentrations and suboxic conditions, whereas the ammonia oxidation (nitrification and nitrifier denitrification) is favored at higher concentrations of ammonia and DO (Quick et al., 2019). Because of the extremely low ammonia concentrations and high DO in the FW, it is not conducive to the production of N_2O through the above two pathways. Finally, in the northeast forested watershed, a high flow rate owing to steep terrain may hinder the production of N_2O. The low flow speeds regions are usually important sites for N_2O production since microbial nitrogen processing requires intermediate residence times (Quick et al., 2019).

3.3. Influences of environmental factors

3.3.1. Relationship between N_2O emissions and riverine physicochemical indicators

Riverine physicochemical characteristics (Table 1) affect N_2O production through biogeochemical or physical processes. As shown in Fig. 6, the physicochemical indicators of the river may be potential proximate controls of N_2O emissions. The Cl^- ($r = 0.80$; $p < 0.001$) was most significantly associated with N_2O emission. On the one hand, Cl^- perhaps stimulated nitrifier activity. The activity of the nitrifier was stimulated by 50% with increasing salinity from 0 to 15 psu (Magalhães et al., 2005). On the other hand, both microbial population and N_2O reductases were sensitive to salinity in freshwater or low-salinity sites (Teixeira et al., 2013). The ammonia-oxidizing archaea (AOA) abundance correlated with salinity and was highest at mid salinity. The study area is located in an inland freshwater watershed with low salinity levels. The abundance of AOA and the potential nitrification rate were significantly and positively correlated with low salinity levels (Beaulieu et al., 2011). Therefore, suitable Cl^- concentrations promote microbial activity and increase microbial diversity, thereby increasing N_2O production in water columns and sediments (Li et al., 2020).

Secondly, N-related indicators (TN, NH_4^+, NO_3^-) can also significantly affect N_2O emissions. The correlation between N_2O emission and NO_3^- ($r = 0.63$; $p < 0.001$) was higher than that of NH_4^+ ($r = 0.40$; $p < 0.001$). The positive correlation between N_2O emissions and NO_3^- might be that higher NO_3^- concentrations suppressed the production of nitrous oxide reductase, an enzyme that reduces N_2O to N_2 (Zhao et al., 2014). In addition to denitrification regulated by NO_3^-, nitrifier denitrification and nitrification are also important processes for the production of N_2O. Higher NH_4^+ concentrations can promote nitrifier activity, increasing NO_3^- concentrations (Quick et al., 2019). This increase in NO_3^- concentrations in turn leads to enhanced denitrification activity. FW, AW and UW represent the different N levels, thus may show different response to riverine dissolved N_2O (Mwanake et al., 2019). Compared with AW and

Table 1
Riverine physicochemical indicators for different watersheds.

Sampling season	Watershed type	TP (mg/L)	TN (mg/L)	NH_4^+ (mg/L)	NO_3^- (mg/L)	SO_4^{2-} (mg/L)	Cl^- (mg/L)	pH	DO (mg/L)	Temperature (°C)
Wet period	FW	0.04 ± 0.05	0.3 ± 0.44	0.05 ± 0.07	1.34 ± 1.23	2.92 ± 1.73	2.54 ± 1.72	7 ± 0.59	7.43 ± 2.02	28.64 ± 2.08
	AW	0.18 ± 0.12	3.4 ± 2.11	1.8 ± 1.68	7.2 ± 7.87	22.24 ± 15.6	24.64 ± 13.62	7.2 ± 0.14	5.65 ± 0.27	29.88 ± 0.44
	UW	0.26 ± 0.12	5.83 ± 1.3	1.76 ± 1.59	12.61 ± 9.13	37.82 ± 21.72	28.16 ± 11.5	7.14 ± 0.2	5.79 ± 0.26	29.02 ± 1.04
	MW	0.12 ± 0.07	1.75 ± 1.1	0.26 ± 0.18	6.94 ± 6.9	57.71 ± 114.4	6.79 ± 4.06	7.23 ± 0.23	6.07 ± 1.04	27.87 ± 0.89
Drier period	FW	0.04 ± 0.05	0.92 ± 0.95	0.06 ± 0.14	3.43 ± 3.08	3.97 ± 1.82	2.95 ± 2.07	7.28 ± 0.24	9.98 ± 1.66	7.41 ± 1.78
	AW	0.1 ± 0.05	2.89 ± 0.89	1.08 ± 1.01	7.47 ± 2.56	24.94 ± 14.43	20.35 ± 10.29	6.81 ± 0.13	8.73 ± 1.69	9.83 ± 1.44
	UW	0.18 ± 0.19	7.38 ± 2.02	1.39 ± 2.01	27.27 ± 10.23	59.12 ± 28.84	63.57 ± 32.87	6.95 ± 0.21	9.1 ± 2.75	13.58 ± 2.54
	MW	0.04 ± 0.06	1.62 ± 1.05	0.33 ± 0.48	5.72 ± 3.55	84.95 ± 164.95	8.15 ± 8.66	7.11 ± 0.19	9.66 ± 2.17	10.77 ± 1.85

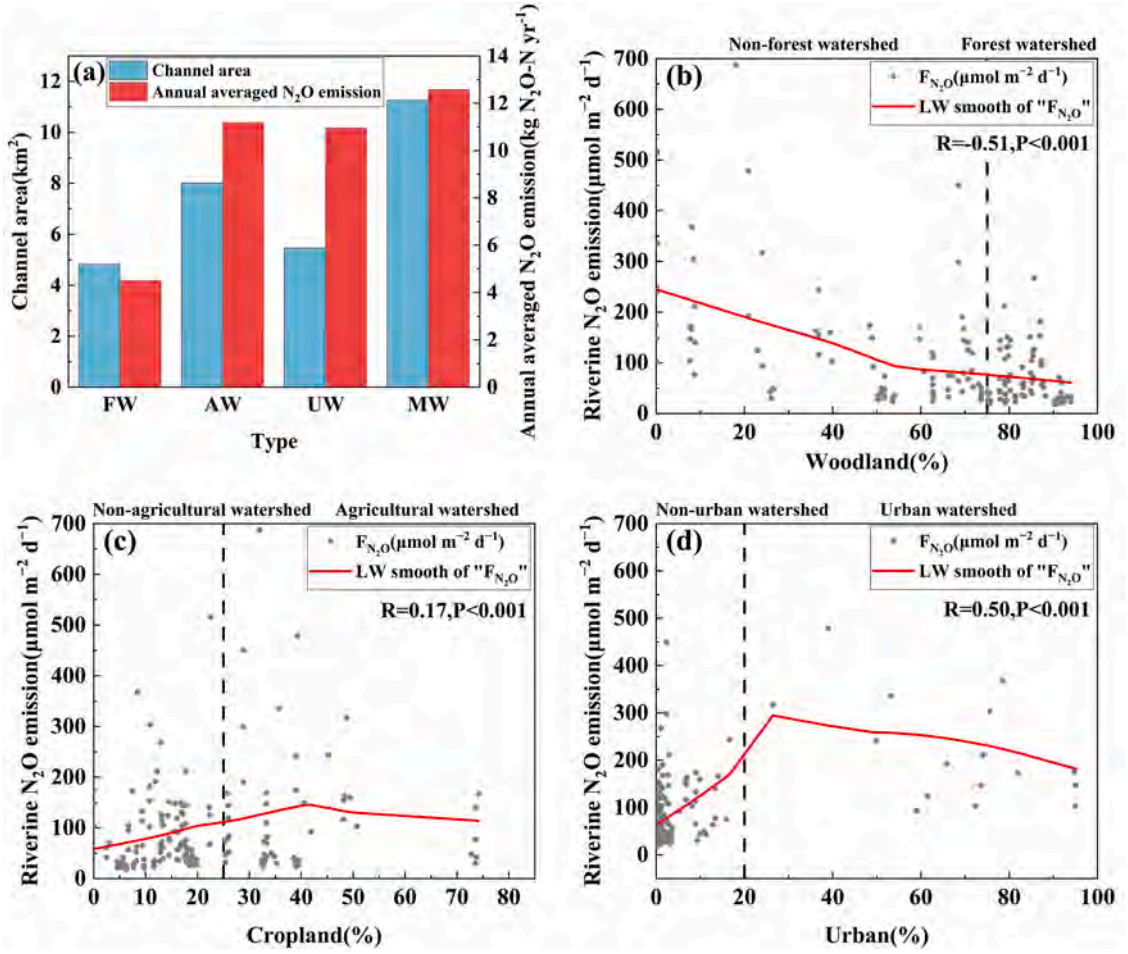

Fig. 5. The relationships between channel area and annual mean N_2O emissions from rivers with different land uses (a). The relationships between modeled monthly mean N_2O emission fluxes from rivers in the subbasin and the percentage of (b) woodland (c) cropland and (d) urban in their subbasin, respectively. Linear regression R values and significance degree are shown. LOWESS fit was used to visually demonstrate the influences of the land use compositions on riverine N_2O fluxes.

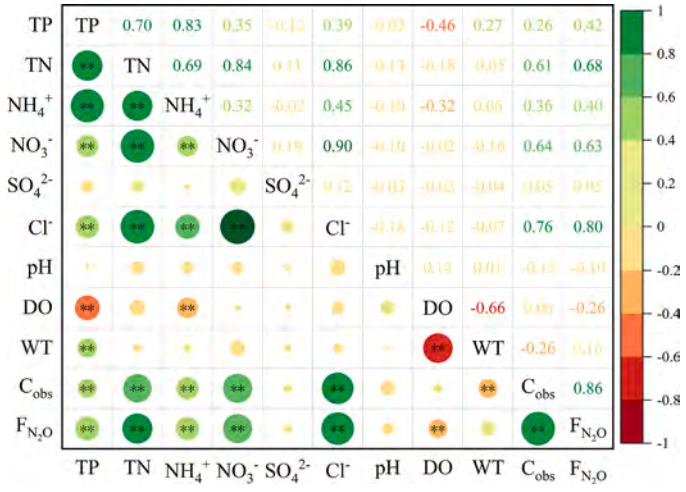

Fig. 6. Matrices of Spearman's correlations between river physicochemical variables and N_2O emission fluxes ($n = 102$;*$p < 0.05$;**$p < 0.01$) .Green and red dots within squares indicate to positive and negative correlations, respectively. The numbers above the diagonal line represent Spearman's correlation coefficients, and their colors match the colors of the corresponding circles.

UW, the dissolved N_2O concentrations in forested rivers responded weakly to DIN (Fig. S6), which suggests that other factors such as DO may also be limiting factors for N_2O generation in addition to N-related indicators (Venkiteswaran et al., 2014).Dissolved N_2O concentrations showed a strong positive correlation with DIN when DIN was less than 12 mg/L in UW (Fig. S6), suggesting that the reactant is an important explanatory variable for N_2O production (Quick et al., 2019).But as the concentration of DIN increased (DIN > 12 mg/L), the reactants concentration approached saturation, and other indicators such as carbon sources and conductivity may play a more important role in N_2O emissions (Turner et al., 2016).

Other physicochemical indicators (TP, DO, water temperature) are also positively related to riverine N_2O emissions. For example, TP ($r = 0.42$; $p < 0.001$) was positively correlated with N_2O emissions, and the correlation was higher than that of NH_4^+ ($r = 0.40$; $p < 0.001$) in this study. For one thing, P loading could relieve the phosphorus-deficiency state of nitrogen-cycling bacteria and affect microbial activities leading to hypoxia in the water environment, promoting the production of N_2O (He et al., 2017). For another thing, N_2O production is affected by phytoplankton biomass, and relatively high TP concentrations have the potential to enhance autotrophic organic carbon and chlorophyll a concentrations (Wang et al., 2021). DO ($r = -0.26$; $p < 0.01$) was negatively related to N_2O emissions in this region. The excessive DO would inhibit anaerobic metabolism and key enzymes that control N_2O reduction and formation. The average DO level in the study area was slightly higher than the suboxic conditions favored by N_2O production, and the small variations (low SD in Table 1) resulted in a weaker

influence than other physicochemical factors (Venkiteswaran et al., 2014).

3.3.2. Relative importance of environmental factors in N_2O emissions

We further determined the relative contributions of different factor types to N_2O emission fluxes (Fig. 7). SEM results indicated that dissolved N_2O concentration played a decisive role in the process of water-air exchange ($r = 0.841$, $p < 0.001$). Spatiotemporal distribution of N_2O emissions followed a similar pattern to riverine dissolved N_2O concentration (Figs. 4b and 6) (Harley et al., 2015; Wang et al., 2015). The correlation analysis also suggested a similar pattern between dissolved N_2O concentrations and riverine N_2O emissions ($r = 0.86$; $p < 0.001$). The key factors influencing the dissolved N_2O concentration were non-point source ($r = 0.678$, $p < 0.001$), point source ($r = 0.241$, $p < 0.01$) and water quality ($r = 0.200$, $p < 0.05$) in sequence. Non-point source impacts are directly attributable to intensive fertilizer use, as well as human and animal waste, resulting in greatly increased nitrogen exports in the drainages, thereby promoting N_2O generation and emissions from aquatic systems (Chen et al., 2015). The results of SEM further emphasized that the cultivation period was the temporal hotspot of riverine N_2O emissions under the influence of non-point sources. There are four possible underlying reasons behind the high N_2O emissions in the downstream urban rivers. Firstly, downstream urban rivers can receive nutrients from midstream agricultural rivers (Zhou et al., 2022). Secondly, the impacts of agricultural non-point sources on rivers are mainly in the overlapping period of fertilization and heavy precipitation. Regardless of the season, the WWTPs discharge sewage steadily. Therefore, the impact cycle of point sources on UW is longer (Chen et al., 2015; Zhou et al., 2022). Then, direct emissions from cropland soil are the major source of regional atmospheric N_2O concentrations (Huang et al., 2022). The higher theoretical equilibrium concentration in the AW suppressed the diffusion effect of riverine N_2O. Finally, the effects of point sources and water quality are more pronounced in UW than in AW. Point sources transport large amounts of nutrients and exogenous dissolved N_2O to urban reaches. At the same time, the suitable water quality of urban rivers is conducive to the production of dissolved N_2O (Zhang et al., 2020, 2021).

Transfer velocity ($r = 0.209$, $p < 0.01$) and theoretical equilibrium N_2O concentration ($r = -0.176$, $p < 0.01$) were secondary factors affecting riverine N_2O emissions. The key factors affecting the transfer velocity were meteorological factors ($r = 0.891$, $p < 0.001$) and land use ($r = 0.308$, $p < 0.001$). Meteorological variables (temperature, precipitation, and evaporation) are the key factors controlling flow and water levels, and water temperature varies regularly with air temperature (Liang et al., 2021). High water velocity, wind speed, and temperature can enhance transfer velocity across the water−air interface. Land use is another important factor affecting the N_2O transfer velocity (Wang et al., 2020). The transfer velocities in FW, AW, and UW are controlled by water velocity, wind speed, and water temperature, respectively. Firstly, the northeast forest watershed has a steep slope and fast flow, while the non-forest watershed has a gentle slope and slow flow (Guan et al., 2020; Zhang et al., 2021). Second, the flat agricultural landscape promoted the gas diffusing effect, while the high-rise buildings in the urban landscape and tall trees in the forest landscape weakened the influence of wind speed on riverine N_2O flux (Song et al., 2022). Finally, the average *in-situ* water temperatures in UW are slightly higher than in others due to warm sewage and urban heat island effects (Venkiteswaran et al., 2014).

The key factors affecting the theoretical equilibrium N_2O concentration were meteorological factors ($r = -0.998$, $p < 0.001$). Air temperature changes in meteorological factors control fugacity changes, thereby affecting the theoretical equilibrium concentration (Gao et al., 2020). The results of SEM also explain, from one side, that N_2O generation by river microbial in this study does not depend on water temperature. N_2O emission is mainly controlled by dissolved N_2O, while water temperature mainly affects the theoretical equilibrium concentration. Therefore, N_2O emission has no statistical correlation with water temperature. On the flip side, the effect of water temperature is concealed by more critical factors (Beaulieu et al., 2010). In this study, the water temperature was negatively related to DO ($r = -0.66$; $p < 0.001$), so variability in DO may overwhelm the control of temperature on microbial metabolism (Fig. 6) (Zhang et al., 2020b).

3.4. Limitations and future research directions

The uncertainties of this study stem from model architecture, parameters, and observational data used for validation and analysis. Firstly, the dissolved N_2O concentration was only calculated based on stream $[NH_4^+]$ and $[NO_3^-]$ in this study, while many other environmental indicators (such as water temperature, DO, riverbed morphology, dissolved organic carbon and particulate, etc.) may also influence its concentration. Although the calculation of the gas transfer velocities takes into account the effects of water temperature and riverbed morphology, the dissolved N_2O concentration model does not reflect the effects of these environmental factors (Fu et al., 2018). In addition, the empirical equation of multiple linear regression has some uncertainties. Linear regression explores the influence of environmental factors on a fixed basis of other factors, without considering the complex interactions of

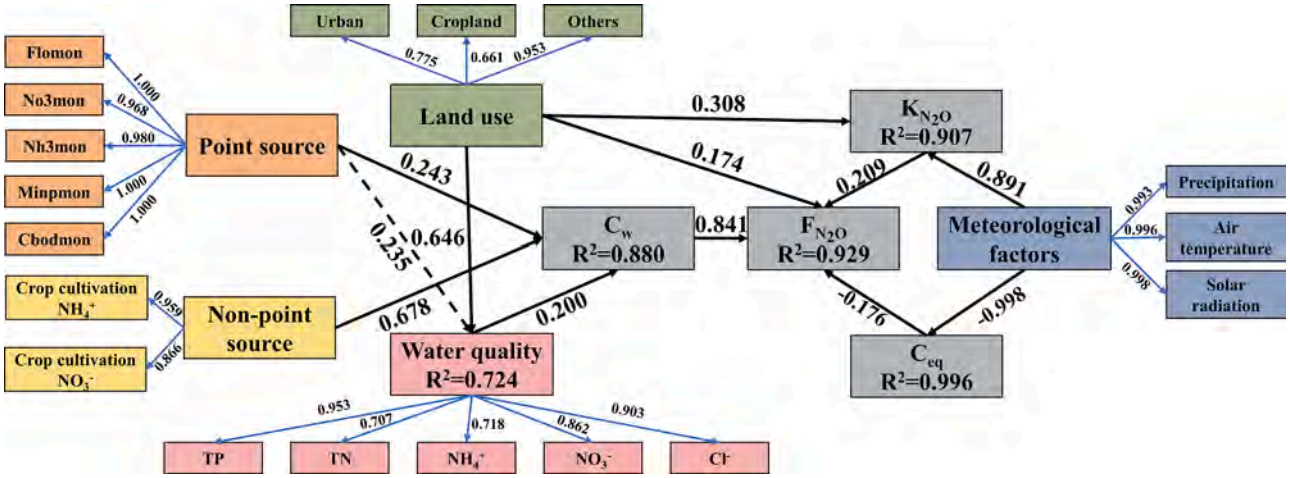

Fig. 7. PLS-SEM framework and model results of the impact of environmental factors on riverine N_2O emissions fluxes. Large and small rectangles represent latent and observed variables, respectively. Black thick solid line and black thick dashed line indicate significant effect ($p < 0.05$) and insignificant effect ($p > 0.05$), respectively. Numbers on thick black and thin blue lines refer path coefficients and indicator loadings, respectively.

environmental factors. And empirical models capture correlation rather than causation (Zhang et al., 2020a). Second, another uncertainty is related to the calculation of k. Here, we adopted Eq. (9) to calculate k. However, the riverine N_2O emissions calculated by different k values under the same environment can also be significantly different. Thus, it remains a great challenge to quantify k under different field conditions and choose the correct parameterization of k to achieve the best estimation (Wang et al., 2020). Third, it is difficult to achieve long-term field trials and monitoring of N_2O emissions in the whole basin due to labor and financial limitations. The limited number of samples may lead to a lack of sufficient explanatory power for spatiotemporal patterns and driving factors. Therefore, an emphasis on greater temporal (higher sampling frequency) and spatial (more locations) data collection is necessary to enhance model usability and interpretability of drivers (Hu et al., 2021b). Finally, this study only explored the relationship between N_2O emissions and basic environmental factors, without considering the contributions of microbial abundance and activity and N_2O production and consumption. Therefore, detailed studies on the microbial processes influencing the N_2O emission process in inland rivers should receive attention in the future (Yang et al., 2020).

4. Conclusion

In this study, we determined the spatiotemporal fluctuations of riverine N_2O emissions based on SWAT outputs and established empirical equations, and evaluated model performance through field measurements. The results show that N_2O emissions from rivers in subtropical inland watersheds have obvious spatiotemporal patterns. Temporally, the high N_2O emissions from the river occurred from August to October (accounting for 35.38% of the annual emission). The diffuse nitrogen loads on the land surface increased sharply due to the effects of plant and fertilization. In the meantime, heavy precipitation events enhanced the transport of nutrients, resulting in increasing nitrogen levels in rivers. Spatially, riverine N_2O emissions fluxes from different types of land use had great spatial heterogeneity, as follows: urban watersheds (191.22 ± 156.19 μmol m^{-2} d^{-1}) > agricultural watersheds (123.48 ± 99.64 μmol m^{-2} d^{-1}) > mixed watersheds (82.25 ± 54.24 μmol m^{-2} d^{-1}) > forest watersheds (63.18 ± 59.40 μmol m^{-2} d^{-1}). The exogenous dissolved N_2O and suitable physical and chemical indicators (sufficient nitrogen supply and relatively low DO conditions) were the reasons for the high N_2O emissions in urban watersheds. In addition, the physicochemical indicators of the river are potential direct controlling factors of N_2O emissions. Riverine N_2O emissions were significantly correlated to Cl^- ($r = 0.80$; $p < 0.001$) and N-related indicators (TN, NO_3^- and NH_4^+). On the one hand, Cl^- perhaps stimulated nitrifier activity. On the other hand, both microbial population and N_2O reductases were sensitive to salinity in freshwater or low-salinity sites. It also emphasized that N-related indicators are important reactants for N_2O generation, which can promote nitrification and denitrification. Meanwhile, SEM revealed that riverine N_2O emissions follow the similar pattern to dissolved N_2O concentrations ($r = 0.841$, $p < 0.001$), and non-point sources ($r = 0.678$, $p < 0.001$) were identified as the most influential variable in riverine dissolved N_2O concentrations. Non-point source impacts lead to greatly increased nitrogen exports in the drainages, thereby promoting N_2O generation and emissions from aquatic systems.

Declaration of Competing Interest

The authors declare no conflict of interest.

Data availability

Data will be made available on request.

Acknowledgments

This work was supported by National Natural Science Foundation of China (51979101, 72088101, 51679082), Hunan Provincial Natural Science Foundation (2019JJ20002), and the Science and Technology Program of the Water Resources Department of Hunan Province (XSKJ2021000-06). We also thank students from Hunan University and Institute of Subtropical Agriculture, Chinese Academy of Sciences for their help in field sample collection and laboratory measurements.

Supplementary materials

Supplementary material associated with this article can be found, in the online version, at doi:10.1016/j.watres.2022.119515.

References

Beaulieu, J.J., Shuster, W.D., Rebholz, J.A., 2010. Nitrous oxide emissions from a large, impounded river: the Ohio River. Environ. Sci. Technol. 44, 7527–7533. https://doi.org/10.1021/es1016735.

Beaulieu, J.J., Tank, J.L., Hamilton, S.K., Wollheim, W.M., Hall, R.O., Mulholland, P.J., Peterson, B.J., Ashkenas, L.R., Cooper, L.W., Dahm, C.N., Dodds, W.K., Grimm, N.B., Johnson, S.L., McDowell, W.H., Poole, G.C., Valett, H.M., Arango, C.P., Bernot, M.J., Burgin, A.J., Crenshaw, C.L., Helton, A.M., Johnson, L.T., O'Brien, J.M., Potter, J.D., Sheibley, R.W., Sobota, D.J., Thomas, S.M., 2011. Nitrous oxide emission from denitrification in stream and river networks. Proc. Natl. Acad. Sci. U. S. A. 108, 214–219. https://doi.org/10.1073/pnas.1011464108.

Bhanja, S.N., Wang, J., Shrestha, N.K., Zhang, X., 2019. Microbial kinetics and thermodynamic (MKT) processes for soil organic matter decomposition and dynamic oxidation-reduction potential: model descriptions and applications to soil N2O emissions. Environ. Pollut. 247, 812–823. https://doi.org/10.1016/j.envpol.2019.01.062.

Borges, A.V., Darchambeau, F., Lambert, T., Bouillon, S., Morana, C., Brouyère, S., Hakoun, V., Jurado, A., Tseng, H.-C., Descy, J.-P., Roland, F.A.E., 2018. Effects of agricultural land use on fluvial carbon dioxide, methane and nitrous oxide concentrations in a large European river, the Meuse (Belgium). Sci. Total Environ. 610–611, 342–355. https://doi.org/10.1016/j.scitotenv.2017.08.047.

Borges, A.V., Darchambeau, F., Teodoru, C.R., Marwick, T.R., Tamooh, F., Geeraert, N., Omengo, F.O., Guérin, F., Lambert, T., Morana, C., Okuku, E., Bouillon, S., 2015. Globally significant greenhouse-gas emissions from African inland waters. Nat. Geosci. 8, 637–642. https://doi.org/10.1038/ngeo2486.

Chen, N., Wu, J., Zhou, X., Chen, Z., Lu, T., 2015. Riverine N_2O production, emissions and export from a region dominated by agriculture in Southeast Asia (Jiulong River). Agric. Ecosyst. Environ. 208, 37–47. https://doi.org/10.1016/j.agee.2015.04.024.

Fu, C., Lee, X., Griffis, T.J., Baker, J.M., Turner, P.A., 2018. A modeling study of direct and indirect N_2O emissions from a representative catchment in the U.S. corn belt. Water Resour. Res. 54, 3632–3653. https://doi.org/10.1029/2017WR022108.

Gao, X., Ouyang, W., Hao, Z., Xie, X., Lian, Z., Hao, X., Wang, X., 2019. SWAT-N_2O coupler: an integration tool for soil N_2O emission modeling. Environ. Model. Softw. 115, 86–97. https://doi.org/10.1016/j.envsoft.2019.02.008.

Gao, X., Ouyang, W., Lin, C., Wang, K., Hao, F., Hao, X., Lian, Z., 2020. Considering atmospheric N_2O dynamic in SWAT model avoids the overestimation of N_2O emissions in river networks. Water Res. 174, 115624 https://doi.org/10.1016/j.watres.2020.115624.

Ghimire, U., Shrestha, N.K., Biswas, A., Wagner-Riddle, C., Yang, W., Prasher, S., Rudra, R., Daggupati, P., 2020. A review of ongoing advancements in soil and water assessment tool (SWAT) for nitrous oxide (N_2O) modeling. Atmosphere 11, 450. https://doi.org/10.3390/atmos11050450.

Grossel, A., Bourennane, H., Ayzac, A., Pasquier, C., Hénault, C., 2021. Indirect emissions of nitrous oxide in a cropland watershed with contrasting hydrology in central France. Sci. Total Environ. 766, 142664 https://doi.org/10.1016/j.scitotenv.2020.142664.

Guan, Y., Lu, H., Yin, C., Xue, Y., Jiang, Y., Kang, Y., He, L., Heiskanen, J., 2020. Vegetation response to climate zone dynamics and its impacts on surface soil water content and albedo in China. Sci. Total Environ. 747, 141537 https://doi.org/10.1016/j.scitotenv.2020.141537.

Hair, J.F., Sarstedt, M., Ringle, C.M., Mena, J.A., 2012. An assessment of the use of partial least squares structural equation modeling in marketing research. J. Acad. Mark. Sci. 40, 414–433. https://doi.org/10.1007/s11747-011-0261-6.

Harley, J.F., Carvalho, L., Dudley, B., Heal, K.V., Rees, R.M., Skiba, U., 2015. Spatial and seasonal fluxes of the greenhouse gases N_2O, CO_2 and CH_4 in a UK macrotidal estuary. Estuar. Coast. Shelf Sci. 153, 62–73. https://doi.org/10.1016/j.ecss.2014.12.004.

He, Y., Wang, X., Chen, H., Yuan, X., Wu, N., Zhang, Y., Yue, J., Zhang, Q., Diao, Y., Zhou, L., 2017. Effect of watershed urbanization on N_2O emissions from the Chongqing metropolitan river network, China. Atmos. Environ. 171, 70–81. https://doi.org/10.1016/j.atmosenv.2017.09.043.

Hellerstein, J.M., 2008. Quantitative data cleaning for large databases 42.

Henseler, J., Ringle, C.M., Sarstedt, M., 2015. A new criterion for assessing discriminant validity in variance-based structural equation modeling. J. Acad. Mark. Sci. 43, 115–135. https://doi.org/10.1007/s11747-014-0403-8.

Hu, M., Chen, D., Dahlgren, R.A., 2016. Modeling nitrous oxide emission from rivers: a global assessment. Glob. Chang. Biol. 22, 3566–3582. https://doi.org/10.1111/gcb.13351.

Hu, M., Li, B., Wu, K., Zhang, Y., Wu, H., Zhou, J., Chen, D., 2021a. Modeling riverine N_2O sources, fates, and emission factors in a typical river network of eastern China. Environ. Sci. Technol. 1c01301. https://doi.org/10.1021/acs.est.1c01301. Acs.EST.

Hu, M., Li, B., Wu, K., Zhang, Y., Wu, H., Zhou, J., Chen, D., 2021b. Modeling riverine N_2O sources, fates, and emission factors in a typical river network of eastern China. Environ. Sci. Technol. acs.est. 1c01301. https://doi.org/10.1021/acs.est.1c01301.

Huang, J., Liu, R., Wang, Q., Gao, X., Han, Z., Gao, J., Gao, H., Zhang, S., Wang, J., Zhang, L., Xia, X., 2022. Climate factors affect N_2O emissions by influencing the migration and transformation of nonpoint source nitrogen in an agricultural watershed. Water Res. 223, 119028 https://doi.org/10.1016/j.watres.2022.119028.

Hulland, J., 1999. Use of partial least squares (PLS) in strategic management research: a review of four recent studies. Strateg. Manag. J. 20, 195–204. https://doi.org/10.1002/(SICI)1097-0266(199902)20:2<195::AID-SMJ13>3.0.CO;2-7.

Jana, M., Sar, N., 2016. Modeling of hotspot detection using cluster outlier analysis and Getis-Ord Gi* statistic of educational development in upper-primary level, India. Model. Earth Syst. Environ. 2, 60. https://doi.org/10.1007/s40808-016-0122-x.

Khan, O., Daddi, T., Iraldo, F., 2021. Sensing, seizing, and reconfiguring: key capabilities and organizational routines for circular economy implementation. J. Clean. Prod. 287, 125565 https://doi.org/10.1016/j.jclepro.2020.125565.

Lan, X., K.W. Thoning, and E.J. Dlugokencky, 2022. Trends in globally-averaged CH4, N2O, and SF6 determined from NOAA global monitoring laboratory measurements.

Li, M., Peng, C., Zhang, K., Xu, L., Wang, J., Yang, Y., Li, P., Liu, Z., He, N., 2021. Headwater stream ecosystem: an important source of greenhouse gases to the atmosphere. Water Res. 190, 116738 https://doi.org/10.1016/j.watres.2020.116738.

Li, Y., Zhang, L., Xue, L., Fan, W., Liu, F., Yang, H., 2020. Spatial variation in aragonite saturation state and the influencing factors in Jiaozhou Bay, China. Water 12, 825. https://doi.org/10.3390/w12030825.

Liang, J., Liu, Q., Zhang, H., Li, Xiaodong, Qian, Z., Lei, M., Li, Xin, Peng, Y., Li, S., Zeng, G., 2020. Interactive effects of climate variability and human activities on blue and green water scarcity in rapidly developing watershed. J. Clean. Prod. 265, 121834 https://doi.org/10.1016/j.jclepro.2020.121834.

Liang, J., Yi, Y., Li, Xiaodong, Yuan, Y., Yang, S., Li, Xin, Zhu, Z., Lei, M., Meng, Q., Zhai, Y., 2021. Detecting changes in water level caused by climate, land cover and dam construction in interconnected river–lake systems. Sci. Total Environ. 788, 147692 https://doi.org/10.1016/j.scitotenv.2021.147692.

Liu, Y., Zhou, Z., Zhang, X., Xu, X., Chen, H., Xiong, Z., 2015. Net global warming potential and greenhouse gas intensity from the double rice system with integrated soil–crop system management: a three-year field study. Atmos. Environ. 116, 92–101. https://doi.org/10.1016/j.atmosenv.2015.06.018.

Magalhães, C.M., Joye, S.B., Moreira, R.M., Wiebe, W.J., Bordalo, A.A., 2005. Effect of salinity and inorganic nitrogen concentrations on nitrification and denitrification rates in intertidal sediments and rocky biofilms of the Douro River estuary, Portugal. Water Res. 39, 1783–1794. https://doi.org/10.1016/j.watres.2005.03.008.

Marzadri, A., Amatulli, G., Tonina, D., Bellin, A., Shen, L.Q., Allen, G.H., Raymond, P.A., 2021. Global riverine nitrous oxide emissions: the role of small streams and large rivers. Sci. Total Environ. 776, 145148 https://doi.org/10.1016/j.scitotenv.2021.145148.

Marzadri, A., Dee, M.M., Tonina, D., Bellin, A., Tank, J.L., 2017. Role of surface and subsurface processes in scaling N_2O emissions along riverine networks. Proc. Natl. Acad. Sci. U. S. A. 114, 4330–4335. https://doi.org/10.1073/pnas.1617454114.

Marzadri, A., Tonina, D., Bellin, A., 2020. Power law scaling model predicts N_2O emissions along the Upper Mississippi River basin. Sci. Total Environ. 732, 138390 https://doi.org/10.1016/j.scitotenv.2020.138390.

Mwanake, R.M., Gettel, G.M., Aho, K.S., Namwaya, D.W., Masese, F.O., Butterbach-Bahl, K., Raymond, P.A., 2019. Land use, not stream order, controls N_2O concentration and flux in the Upper Mara River Basin, Kenya. JGR Biogeosci. 124, 3491–3506. https://doi.org/10.1029/2019JG005063.

Qin, X., Li, Yu'e, Wan, Y., Fan, M., Liao, Y., Li, Yong, Wang, B., Gao, Q., 2020. Diffusive flux of CH_4 and N_2O from agricultural river networks: regression tree and importance analysis. Sci. Total Environ. 717, 137244 https://doi.org/10.1016/j.scitotenv.2020.137244.

Quick, A.M., Reeder, W.J., Farrell, T.B., Tonina, D., Feris, K.P., Benner, S.G., 2019. Nitrous oxide from streams and rivers: a review of primary biogeochemical pathways and environmental variables. Earth Sci. Rev. 191, 224–262. https://doi.org/10.1016/j.earscirev.2019.02.021.

Quick, A.M., Reeder, W.J., Farrell, T.B., Tonina, D., Feris, K.P., Benner, S.G., 2016. Controls on nitrous oxide emissions from the hyporheic zones of streams. Environ. Sci. Technol. 50, 11491–11500. https://doi.org/10.1021/acs.est.6b02680.

Raymond, P.A., Zappa, C.J., Butman, D., Bott, T.L., Potter, J., Mulholland, P., Laursen, A. E., McDowell, W.H., Newbold, D., 2012. Scaling the gas transfer velocity and hydraulic geometry in streams and small rivers: gas transfer velocity and hydraulic geometry. Limnol. Oceanogr. 2, 41–53. https://doi.org/10.1215/21573689-1597669.

Shrestha, N.K., Thomas, B.W., Du, X., Hao, X., Wang, J., 2018. Modeling nitrous oxide emissions from rough fescue grassland soils subjected to long-term grazing of different intensities using the soil and water assessment tool (SWAT). Environ. Sci. Pollut. Res. 25, 27362–27377. https://doi.org/10.1007/s11356-018-2719-2.

Song, K., Senbati, Y., Li, L., Zhao, X., Xue, Y., Deng, M., 2022. Distinctive microbial processes and controlling factors related to indirect N_2O emission from agricultural and urban rivers in Taihu Watershed. Environ. Sci. Technol. 56, 4642–4654. https://doi.org/10.1021/acs.est.1c07980.

Soued, C., del Giorgio, P.A., Maranger, R., 2016. Nitrous oxide sinks and emissions in boreal aquatic networks in Québec. Nat. Geosci. 9, 116–120. https://doi.org/10.1038/ngeo2611.

Teixeira, C., Magalhães, C., Joye, S.B., Bordalo, A.A., 2013. The role of salinity in shaping dissolved inorganic nitrogen and N_2O dynamics in estuarine sediment–water interface. Mar. Pollut. Bull. 66, 225–229. https://doi.org/10.1016/j.marpolbul.2012.11.004.

Tian, H., Xu, R., Canadell, J.G., Thompson, R.L., Winiwarter, W., Suntharalingam, P., Davidson, E.A., Ciais, P., Jackson, R.B., Janssens-Maenhout, G., Prather, M.J., Regnier, P., Pan, N., Pan, S., Peters, G.P., Shi, H., Tubiello, F.N., Zaehle, S., Zhou, F., Arneth, A., Battaglia, G., Berthet, S., Bopp, L., Bouwman, A.F., Buitenhuis, E.T., Chang, J., Chipperfield, M.P., Dangal, S.R.S., Dlugokencky, E., Elkins, J.W., Eyre, B. D., Fu, B., Hall, B., Ito, A., Joos, F., Krummel, P.B., Landolfi, A., Laruelle, G.G., Lauerwald, R., Li, W., Lienert, S., Maavara, T., MacLeod, M., Millet, D.B., Olin, S., Patra, P.K., Prinn, R.G., Raymond, P.A., Ruiz, D.J., van der Werf, G.R., Vuichard, N., Wang, J., Weiss, R.F., Wells, K.C., Wilson, C., Yang, J., Yao, Y., 2020. A comprehensive quantification of global nitrous oxide sources and sinks. Nature 586, 248–256. https://doi.org/10.1038/s41586-020-2780-0.

Turner, P.A., Griffis, T.J., Baker, J.M., Lee, X., Crawford, J.T., Loken, L.C., Venterea, R.T., 2016. Regional-scale controls on dissolved nitrous oxide in the Upper Mississippi River. Geophys. Res. Lett. 43, 4400–4407. https://doi.org/10.1002/2016GL068710.

Urbach, N., Ahlemann, F., 2010. Structural equation modeling in information systems research using partial least squares 11, 37.

Venkiteswaran, J.J., Rosamond, M.S., Schiff, S.L., 2014. Nonlinear response of riverine N_2O fluxes to oxygen and temperature. Environ. Sci. Technol. 48, 1566–1573. https://doi.org/10.1021/es500069j.

Wagena, M.B., Bock, E.M., Sommerlot, A.R., Fuka, D.R., Easton, Z.M., 2017. Development of a nitrous oxide routine for the SWAT model to assess greenhouse gas emissions from agroecosystems. Environ. Model. Softw. 89, 131–143. https://doi.org/10.1016/j.envsoft.2016.11.013.

Wang, G., Wang, J., Xia, X., Zhang, L., Zhang, S., McDowell, W.H., Hou, L., 2018. Nitrogen removal rates in a frigid high-altitude river estimated by measuring dissolved N_2 and N_2O. Sci. Total Environ. 645, 318–328. https://doi.org/10.1016/j.scitotenv.2018.07.090.

Wang, G., Xia, X., Liu, S., Zhang, S., Yan, W., McDowell, W.H., 2021. Distinctive patterns and controls of nitrous oxide concentrations and fluxes from urban inland waters. Environ. Sci. Technol. 55, 8422–8431. https://doi.org/10.1021/acs.est.1c00647.

Wang, J., Chen, N., Yan, W., Wang, B., Yang, L., 2015. Effect of dissolved oxygen and nitrogen on emission of N_2O from rivers in China. Atmos. Environ. 103, 347–356. https://doi.org/10.1016/j.atmosenv.2014.12.054.

Wang, J., Wang, G., Zhang, S., Xin, Y., Jiang, C., Liu, S., He, X., McDowell, W.H., Xia, X., 2022. Indirect nitrous oxide emission factors of fluvial networks can be predicted by dissolved organic carbon and nitrate from local to global scales. Glob. Chang. Biol. 28, 7270–7285. https://doi.org/10.1111/gcb.16458.

Wang, R., Zhang, H., Zhang, W., Zheng, X., Butterbach-Bahl, K., Li, S., Han, S., 2020. An urban polluted river as a significant hotspot for water–atmosphere exchange of CH_4 and N_2O. Environ. Pollut. 264, 114770 https://doi.org/10.1016/j.envpol.2020.114770.

Weiss, R.F., Price, B.A., 1980. Nitrous oxide solubility in water and seawater. Mar. Chem. 8, 347–359. https://doi.org/10.1016/0304-4203(80)90024-9.

Wu, Y., Liu, S., Qiu, L., Sun, Y., 2016. SWAT-DayCent coupler: An integration tool for simultaneous hydro-biogeochemical modeling using SWAT and DayCent. Environ. Model. Softw. 86, 81–90. https://doi.org/10.1016/j.envsoft.2016.09.015.

Yan, Xing, Han, H., Qiu, J., Zhang, L., Xia, Y., Yan, Xiaoyuan, 2022. Suburban agriculture increased N levels but decreased indirect N_2O emissions in an agricultural-urban gradient river. Water Res. 220, 118639 https://doi.org/10.1016/j.watres.2022.118639.

Yang, P., Yang, H., Lai, D.Y.F., Guo, Q., Zhang, Y., Tong, C., Xu, C., Li, X., 2020. Large contribution of non-aquaculture period fluxes to the annual N_2O emissions from aquaculture ponds in Southeast China. J. Hydrol. 582, 124550 https://doi.org/10.1016/j.jhydrol.2020.124550.

Yang, Q., Zhang, X., Abraha, M., Del grosso, S., Robertson, G.P., Chen, J., 2017. Enhancing the soil and water assessment tool model for simulating N_2O emissions of three agricultural systems. Ecosyst. Health Sustain. 3, e01259. https://doi.org/10.1002/ehs2.1259.

Yang, X., Liu, Q., Fu, G., He, Y., Luo, X., Zheng, Z., 2016. Spatiotemporal patterns and source attribution of nitrogen load in a river basin with complex pollution sources. Water Res. 94, 187–199. https://doi.org/10.1016/j.watres.2016.02.040.

Yao, Y., Tian, H., Shi, H., Pan, S., Xu, R., Pan, N., Canadell, J.G., 2020. Increased global nitrous oxide emissions from streams and rivers in the Anthropocene. Nat. Clim. Chang. 10, 138–142. https://doi.org/10.1038/s41558-019-0665-8.

Yu, S., Lu, H., 2018. Relationship between urbanisation and pollutant emissions in transboundary river basins under the strategy of the belt and road initiative. Chemosphere 203, 11–20. https://doi.org/10.1016/j.chemosphere.2018.03.172.

Zhang, W., Li, H., Xiao, Q., Jiang, S., Li, X., 2020a. Surface nitrous oxide (N_2O) concentrations and fluxes from different rivers draining contrasting landscapes: Spatio-temporal variability, controls, and implications based on IPCC emission factor. Environ. Pollut. 263, 114457 https://doi.org/10.1016/j.envpol.2020.114457.

Zhang, W., Li, H., Xiao, Q., Li, X., 2021. Urban rivers are hotspots of riverine greenhouse gas (N_2O, CH_4, CO_2) emissions in the mixed-landscape chaohu lake basin. Water Res. 189, 116624 https://doi.org/10.1016/j.watres.2020.116624.

Zhang, X., Zhi, X., Chen, L., Shen, Z., 2020b. Spatiotemporal variability and key influencing factors of river fecal coliform within a typical complex watershed. Water Res. 178, 115835 https://doi.org/10.1016/j.watres.2020.115835.

Zhao, B., Zhang, Q., 2021. N_2O emission and its influencing factors in subtropical streams, China. Ecol. Process. 10, 54. https://doi.org/10.1186/s13717-021-00307-3.

Zhao, Y., Xia, Y., Li, B., Yan, X., 2014. Influence of environmental factors on net N_2 and N_2O production in sediment of freshwater rivers. Environ. Sci. Pollut. Res. 21, 9973–9982. https://doi.org/10.1007/s11356-014-2908-6.

Zhou, Y., Toyoda, R., Suenaga, T., Aoyagi, T., Hori, T., Terada, A., 2022. Low nitrous oxide concentration and spatial microbial community transition across an urban river affected by treated sewage. Water Res. 216, 118276 https://doi.org/10.1016/j.watres.2022.118276.